iJRASET
International Journal For Research in Applied Science and Engineering Technology

INTERNATIONAL JOURNAL FOR RESEARCH

IN APPLIED SCIENCE & ENGINEERING TECHNOLOGY

Volume: 13 **Issue:** III **Month of publication:** March 2025

DOI: https://doi.org/10.22214/ijraset.2025.67257

www.ijraset.com

Call: 08813907089 | E-mail ID: ijraset@gmail.com

International Journal for Research in Applied Science & Engineering Technology (IJRASET)
ISSN: 2321-9653; IC Value: 45.98; SJ Impact Factor: 7.538
Volume 13 Issue III Mar 2025- Available at www.ijraset.com

Chest X-ray Image Super-Resolution Using Artificial Intelligence

Ayush Patel[1], Prof. (Dr.) Tejas Shah[2]
[1]*Ayush Patel, Research Scholar, Instrumentation & Control Dept., L.D. College of Engineering, Ahmedabad, Gujarat, India*
[2]*Prof. (Dr.) Tejas Shah, Associate Professor, Instrumentation & Control Dept., L.D. College of Engineering, Ahmedabad, Gujarat, India*

Abstract: ***Chest X-ray (CXR) imaging is essential for diagnosing respiratory diseases like pneumonia, but low-resolution (LR) images can make detection less accurate. This study explores how deep learning-based super-resolution (SR) techniques can improve CXR image quality and enhance automated pneumonia detection. Real-ESRNet utilized as the generator to restore image details and Real-ESRGAN NetD as the discriminator to refine structures. The model was fine-tuned on 4,500 images, including original and multi-scale variations, randomly selected from the Random sample of NIH Chest X-ray Dataset, which contains 5,606 labeled images. Training was conducted with a batch size of 10 per GPU for four epochs, totalling 3,240 iterations, with checkpoints saved every 810 iterations. To evaluate the impact of SR, The enhanced images were tested using a classification model based on SqueezeNet embeddings and a neural network in Orange Data Mining software. Results showed that SR-improved images led to better pneumonia detection accuracy compared to LR images, though further optimization is needed for better reconstruction quality. These findings highlight how AI-driven super-resolution can play a significant role in improving medical imaging and automated disease diagnosis.***

Keywords: Chest X-ray image super resolution, Pneumonia classification, Data mining tool, Deep learning, Medical imaging

I. INTRODUCTION

Low-resolution (LR) X-ray imaging is one of the biggest medical diagnosis problems, particularly in the diagnosis of diseases like pneumonia. Edge blurring and loss of high-frequency details in LR images can lead to interference with correct interpretation, where it is difficult for machine learning AI models to detect normal and abnormal cases. These have to be overcome in order to enhance the effectiveness of AI-assisted medical image analysis. The research assesses the effect of AI-super-resolution (SR) on diagnosing pneumonia. The key contributions include fine-tuning of a super-resolution model by utilizing Real-ESRNet as a generator and Real-ESRGAN NetD as a discriminator. The low-resolution (LR) chest X-ray images were four times downscaled, and SR improvement was implemented for better improvement of image quality. Enhanced images were employed in the pneumonia classification with the SqueezeNet embeddings and the neural network from Orange Data Mining software. The research compares performance for SR with classification accuracy, image quality factors like PSNR, SSIM, and MSE, and confusion matrices.

II. RESEARCH WORKFLOW AND METHODOLOGY

The research continues systematically, first fine-tuning SR model on 4,500 diversified original and multi-scale images. The trained model is utilized to upscale the downsampled images and generate high-resolution outputs. LR and SR datasets are utilized to classify pneumonia, and performance is quantitatively analysed and compared graphically.

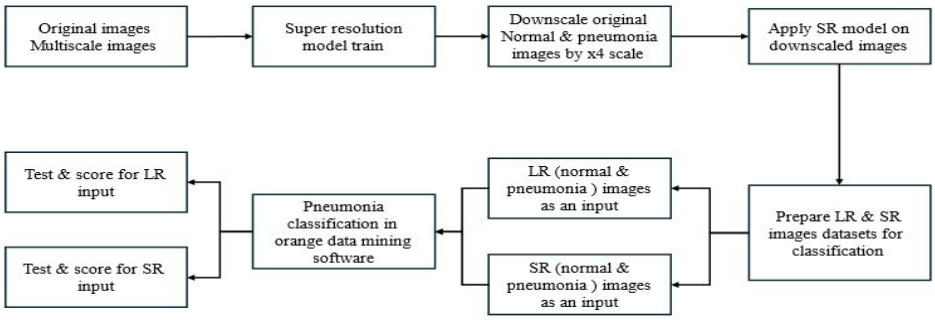

Fig. 1 Proposed Methodology

With AI-based super-resolution, the research enhances the CXR image quality to enable better automatic detection of pneumonia and reduced health care expenditure.

III. RELATED WORK

A. Real-ESRGAN and Real-ESRNet Architecture

Deep learning-based super-resolution enhances medical imaging by reconstructing high-frequency details from low-res (LR) input. Real-ESRGAN builds upon ESRGAN with an RRDB generator and U-Net-based discriminator, optimized with spectral normalization for improved texture realism.

Unlike ESRGAN, Real-ESRGAN works better for handling real-world degradation artifacts, making it potential for application in medical imaging. A variant that omits adversarial training, Real-ESRNet, produces stable reconstructions of high fidelity, critical for clinical applications.

B. Super-Resolution Techniques in Medical Imaging

These three approaches are based on categorical super-resolution (SR): CNN-based, residual learning-based, and GAN-based. CNN models, including SRCNN and FSRCNN, map LR to HR without yielding fine details in higher resolution. Residual networks VDSR and EDSR improve fidelity but are slightly expensive in terms of computational resources. GAN models such as SRGAN and ESRGAN enhance perceptual quality along with their tendency to include artifacts.

Table. 1 Various SR Models and Their Features

Method	Key Features
Bicubic Interpolation	Traditional upscaling approach
SRCNN (Super-Resolution CNN)	Faster version of SRCNN with deconvolution layers
VDSR (Very Deep SR Network)	Deeper CNN, residual learning for better feature extraction
ESRGAN (Enhanced SR GAN)	Uses adversarial training and RRDB blocks for sharp details
Real-ESRGAN	Handles real-world degradations, improves perceptual quality
EDSR (Enhanced Deep SR)	High-performance SR model, removes batch normalization
RDN (Residual Dense Network)	Dense feature extraction, improved texture reconstruction
DRLN (Deep Recursive LR Network)	Efficient recursive learning, reduces memory usage
SwinIR (Swin Transformer for SR)	Transformer-based SR, state-of-the-art image enhancement

SR methods based on transformer networks perform long-range feature extraction but remain less explored in the field of medical imaging due to their high training costs.

C. SqueezeNet for Efficient Feature Extraction

SqueezeNet was selected for pneumonia detection on grounds of its compact architecture vastly reducing computational overheads while retaining classification accuracy. It efficiently compresses feature maps through Fire modules for much faster inference, thus ideal for real-time medical applications. In terms of inference speed, compared with ResNet and DenseNet, SqueezeNet meets performance goals while efficiently handling memory constraints, making it particularly suited for healthcare settings existing under resource limitations, such as portable X-ray imaging systems.

IV. METHODOLOGY

A. *Super-Resolution model*

1) *GPU Specifications*

For training and inference, the NVIDIA T4 GPU provided by Google Colab was utilized. The T4 GPU is a Turing architecture-based accelerator optimized for deep learning tasks.

Table. 2 NVIDIA T4 GPU Specifications

Specification	Value
GPU Architecture	Turing
CUDA Cores	2560
Tensor Cores	320
Memory	16GB GDDR6
Memory Bandwidth	320 GB/s
FP32 Performance	~8.1 TFLOPS
FP16 Performance	~65 TFLOPS (Tensor Cores)
Power Consumption	70W

The NVIDIA T4 is widely used in cloud-based AI applications due to its efficient performance, low power consumption, and optimized support for deep learning workloads.

2) *Fine-Tuning Steps for Super-Resolution Model*

This section covers the fine-tuning steps followed for the super-resolution model. Detailed parameter settings, dataset information, and evaluation metrics are provided in the following sections.

a) Navigate to Working Directory

%cd /content/drive/MyDrive/REAL ESRGAN

The working directory is set to the location where Real-ESRGAN and dataset files are stored in Google Drive.

b) Clone Real-ESRGAN Repository

!git clone https://github.com/xinntao/Real-ESRGAN.git

The official Real-ESRGAN repository is cloned from GitHub to access necessary scripts and model files for training and inference to our google drive

c) Install Dependencies

Essential libraries like basicsr (for training and inference), facexlib, and gfpgan (for face enhancement) are installed. The setup.py develop command ensures the environment is set up correctly.

```
[ ]  # Install basicsr - https://github.com/xinntao/BasicSR
     # We use BasicSR for both training and inference
     !pip install --use-pep517
     !pip install basicsr
     # facexlib and gfpgan are for face enhancement
     !pip install facexlib
     !pip install gfpgan
     !pip install -r requirements.txt
     !python setup.py develop
```

```
Collecting basicsr
  Downloading basicsr-1.4.2.tar.gz (172 kB)
     ━━━━━━━━━━━━━━━━━━━━━━━━━━━━━━━━━━━━━━━━ 172.5/172.5 kB 5.3 MB/s eta 0:00:00
  Preparing metadata (setup.py) ... done
Collecting addict (from basicsr)
  Downloading addict-2.4.0-py3-none-any.whl.metadata (1.0 kB)
Requirement already satisfied: future in /usr/local/lib/python3.10/dist-packages (from basicsr) (1.0.0)
Collecting lmdb (from basicsr)
  Downloading lmdb-1.5.1-cp310-cp310-manylinux_2_17_x86_64.manylinux2014_x86_64.whl.metadata (1.1 kB)
Requirement already satisfied: numpy>=1.17 in /usr/local/lib/python3.10/dist-packages (from basicsr) (1.26.4)
Requirement already satisfied: opencv-python in /usr/local/lib/python3.10/dist-packages (from basicsr) (4.10.0.84)
Requirement already satisfied: Pillow in /usr/local/lib/python3.10/dist-packages (from basicsr) (11.0.0)
Requirement already satisfied: pyyaml in /usr/local/lib/python3.10/dist-packages (from basicsr) (6.0.2)
Requirement already satisfied: requests in /usr/local/lib/python3.10/dist-packages (from basicsr) (2.32.3)
Requirement already satisfied: scikit-image in /usr/local/lib/python3.10/dist-packages (from basicsr) (0.24.0)
```

Fig. 2 Installation of Dependencies

d) Generate Multiscale Images

```
!python scripts/generate_multiscale_DF2K.py --input dataset/pneumonia/HDtrain --output dataset/pneumonia/HDmultiscale
```

A script is executed to create multiscale images from the original dataset, helping the model learn super-resolution at different scales.

e) Generate metadata for training

```
!python scripts/generate_meta_info.py --input dataset/pneumonia/HDtrain dataset/pneumonia/HDmultiscale --root
dataset/pneumonia dataset/pneumonia --meta_info dataset/pneumonia/meta_info.txt
```

This script for generating a metadata file which contains all original and multiscale images file name with folder paths needed for training

f) Train the Model

```
!python realesrgan/train.py -opt options/finetune_realesrgan_x4plus.yml --auto_resume
```

```
!python realesrgan/train.py -opt options/finetune_realesrgan_x4plus.yml --auto_resume
2024-12-18 12:03:30.945865: I tensorflow/core/platform/cpu_feature_guard.cc:210] This TensorFlow binary is optimized to use available CPU instructions
To enable the following instructions: AVX2 AVX512F FMA, in other operations, rebuild TensorFlow with the appropriate compiler flags.
2024-12-18 12:03:32.080912: W tensorflow/compiler/tf2tensorrt/utils/py_utils.cc:38] TF-TRT Warning: Could not find TensorRT
2024-12-18 12:03:33,768 INFO: Dataset [RealESRGANDataset] - pneumonia is built.
/usr/local/lib/python3.10/dist-packages/torch/utils/data/dataloader.py:617: UserWarning: This DataLoader will create 5 worker processes in total. Our
  warnings.warn(
2024-12-18 12:03:33,772 INFO: Training statistics:
        Number of train images: 4500
        Dataset enlarge ratio: 1
        Batch size per gpu: 10
        World size (gpu number): 1
        Require iter number per epoch: 450
        Total epochs: 8; iters: 3240.
2024-12-18 12:03:34,322 INFO: Network [RRDBNet] is created.
2024-12-18 12:03:34,643 INFO: Network: RRDBNet, with parameters: 16,697,987
2024-12-18 12:03:34,644 INFO: RRDBNet(
  (conv_first): Conv2d(3, 64, kernel_size=(3, 3), stride=(1, 1), padding=(1, 1))
  (body): Sequential(
    (0): RRDB(
      (rdb1): ResidualDenseBlock(
        (conv1): Conv2d(64, 32, kernel_size=(3, 3), stride=(1, 1), padding=(1, 1))
```

Fig. 3 Fine Tuning the Model

The training script is executed with a modified `finetune_realesrgan_x4plus.yml` file, which contains fine-tuning parameters. The model learns to generate high-resolution images from low-resolution inputs. For training runtime type selected to T4 GPU.

g) Test Fine-Tuned Model

```
!python inference_realesrgan.py --model_path experiments/pretrained_models/RealESRGAN_x4plus.pth --input inputs
```

The fine-tuned model weights (`net_g_latest.pth`) are moved to the pre-trained models folder and renamed to `RealESRGAN_x4plus.pth`. The inference script processes input images, generating super-resolution outputs stored in the `results` folder.

3) Dataset Details and Analysis

A subset of 900 images selected from the "Random Sample of NIH Chest X-ray Dataset" This is a random sample (5%) of the full dataset which contains 5,606 images sampled from the original NIH Chest X-ray Dataset

Selected Subset Characteristics

a) Total Images: 900
b) Most common age groups: 56Y , 60Y , 51Y
c) Gender Distribution: Male: 496 & Female: 404
d) View Positions: PA (Posterior-Anterior): 531 images & AP (Anterior-Posterior): 369 images
e) No Finding: 462 images
f) Most common abnormalities : Infiltration, Effusion , Atelectasis , Pneumothorax , Consolidation

4) Hyperparameter Settings for Fine-Tuning

This section presents the selected hyperparameter settings used for fine-tuning the super-resolution model. These parameters influence the training process and model performance.

Table. 3 Fine-Tuning Settings for the Model

Parameter	Setting
Model	Real-ESRGAN (Generator: Real-ESRNet, Discriminator: Real-ESRGAN)
Scale Factor	4×
Total Iterations	3240
GT Size	256×256
Generator	RRDBNet (23 Blocks, 64 Features)
Discriminator	UNetDiscriminatorSN (Skip Connection: Yes)
Pretrained Models	RealESRNet_x4plus.pth (G), RealESRGAN_x4plus_netD.pth (D)
Optimizer	Adam (LR: 1e-4, Betas: [0.9, 0.99])
Loss Functions	L1 Loss, Perceptual Loss (VGG19), GAN Loss
Data Augmentation	Horizontal Flip: Yes, Rotation: No, Gaussian Noise: 50%, JPEG Compression: [30, 95]
Logging	Checkpoints every 810 iterations

B. Pneumonia Detection Model in Orange

Orange Data Mining is an open-source and very much user-friendly machine learning and data visualization tool that provides a solid platform for data analysis. It supports classification, clustering, and deep learning workflows according to the visual programming methodology. For this study, Orange will be used to train a pneumonia detection model based on features taken from chest X-ray images and apply the neural network for classification.

1) Pneumonia Classification Workflow in Orange Data Mining

The pneumonia classification workflow in Orange Data Mining seeks to compare how low-resolution (LR) and super-resolution (SR) images perform in detecting pneumonia. The workflow comprises a chain of interconnected components, including image embedding, data merging, neural network training, and evaluation itself. There are set up two pipelines: one with pneumonia classification based on LR images and another one based on SR images. The evaluation of such results as accuracy and other performance metrics is provided through confusion matrices and distribution plots.

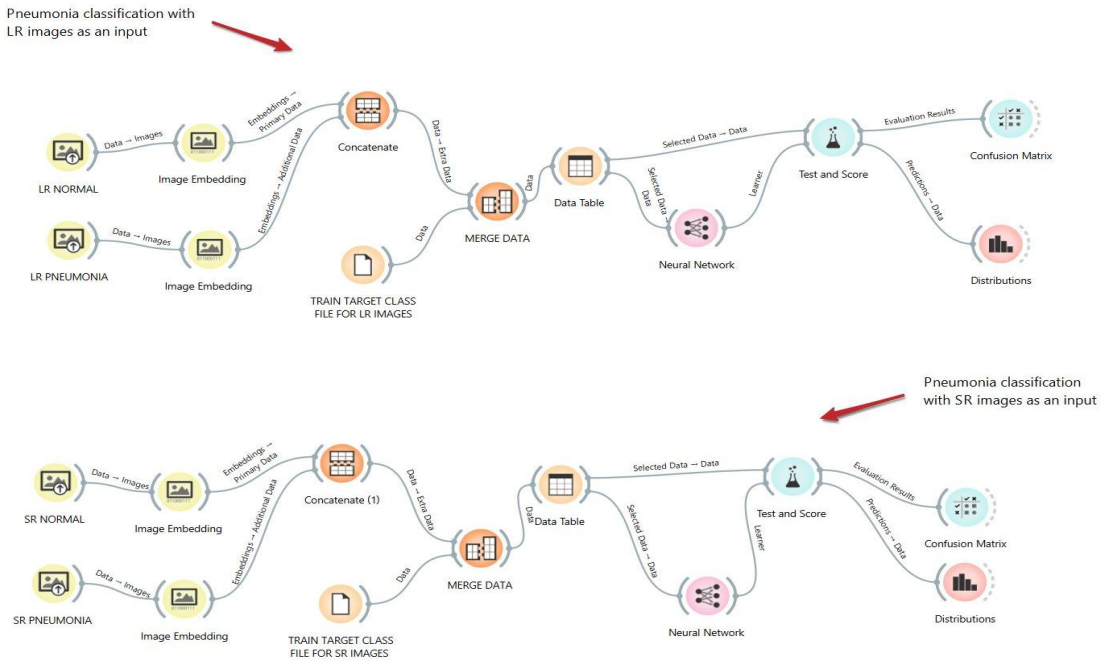

Fig. 4 Model Workflow in Orange Data Mining Tool

2) Image Embedding Process

Image embedding is one of the crucial steps taken in the workflow in which chest X-ray images are transformed into feature vectors using pre-trained deep learning models. In this study, SqueezeNet was used within Orange Data Mining for embedding. SqueezeNet is a powerful deep learning model intended to allow for effective feature extraction, sufficient even for lightweight deployment. The model extracts the meaningful patterns in the image and leads to dimensionality reduction that allows useful data for classification to build a pneumonia detection model. It serves as the training input for this pneumonia classification model, allowing the model to learn appropriate features from images without any pixel-based processing.

hidden origin type	image name	image ownloads/MODEL TEST DATA/image	size	width	height	n0 True	n1 True	n2 True	n3 True	n4 True	n5 True
1	IM-0001-0001	IM-0001-0001.jpeg	46034	464	329	3.68442	2.41808	10.5443	8.10922	7.22382	3.97843
2	IM-0003-0001	IM-0003-0001.jpeg	56416	527	377	3.54403	5.82303	8.10281	7.18524	7.38222	2.74454
3	IM-0005-0001	IM-0005-0001.jpeg	70100	507	459	3.43278	3.3756	9.46398	7.65378	6.85995	2.5612
4	IM-0006-0001	IM-0006-0001.jpeg	43465	415	331	3.46447	3.55663	7.03871	4.89024	4.8991	3.31883
5	IM-0007-0001	IM-0007-0001.jpeg	70480	513	454	4.15973	3.84056	7.93316	7.39524	5.40458	2.28345
6	IM-0009-0001	IM-0009-0001.jpeg	49287	463	360	5.0327	6.13886	7.32211	7.40921	5.89137	3.14861
7	IM-0010-0001	IM-0010-0001.jpeg	51217	468	369	3.5713	4.55436	10.1014	7.22088	7.44568	4.03556
8	IM-0011-0001-...	IM-0011-0001-0001.jpeg	76811	536	479	3.59638	4.16241	10.2431	7.97858	5.9308	1.87198
9	IM-0011-0001-...	IM-0011-0001-0002.jpeg	76386	553	486	3.34156	4.74789	10.276	7.2925	6.60222	2.12424
10	IM-0011-0001	IM-0011-0001.jpeg	62308	465	446	3.19957	6.23877	5.08951	4.98005	5.82583	3.63006
11	IM-0013-0001	IM-0013-0001.jpeg	99418	611	538	3.56434	3.19213	13.259	7.82546	7.30258	4.12947
12	IM-0015-0001	IM-0015-0001.jpeg	44400	450	309	3.02897	3.71917	10.1306	7.90408	4.88972	3.14401
13	IM-0016-0001	IM-0016-0001.jpeg	90268	624	514	2.76039	3.53917	10.5299	8.37909	6.48144	2.88112
14	IM-0017-0001	IM-0017-0001.jpeg	57833	496	389	3.98755	2.18325	7.56126	6.9677	5.29772	1.9788
15	IM-0019-0001	IM-0019-0001.jpeg	50560	479	358	4.44822	2.70134	9.82082	8.112	6.4772	3.62523
16	IM-0021-0001	IM-0021-0001.jpeg	81807	656	473	2.79206	1.70445	9.52396	7.63877	4.72249	4.15462
17	IM-0022-0001	IM-0022-0001.jpeg	14570	325	154	3.1216	3.49795	5.15768	6.61313	3.14758	4.76347
18	IM-0023-0001	IM-0023-0001.jpeg	52865	505	346	1.97382	3.37476	10.1026	7.12111	4.39102	2.80338
19	IM-0025-0001	IM-0025-0001.jpeg	114063	680	614	3.50142	6.17253	12.312	10.1045	5.88078	3.16903
20	IM-0027-0001	IM-0027-0001.jpeg	74032	567	456	2.77878	3.88935	8.73666	7.37162	5.46053	1.92868
21	IM-0028-0001	IM-0028-0001.jpeg	92450	630	531	4.64114	5.82525	11.435	8.76577	7.7019	4.61362
22	IM-0029-0001	IM-0029-0001.jpeg	94145	585	534	2.6811	1.06875	10.8601	9.01974	3.50879	3.24956
23	IM-0030-0001	IM-0030-0001.jpeg	42189	411	328	4.65181	5.12472	9.36833	9.9609	7.98298	2.37838
24	IM-0031-0001	IM-0031-0001.jpeg	60108	487	408	2.99062	2.31027	9.12367	7.4117	3.89031	0.666366
25	IM-0033-0001-...	IM-0033-0001-0001.jpeg	78977	542	488	5.07907	2.82694	11.393	6.47847	6.5608	3.45554
26	IM-0033-0001-...	IM-0033-0001-0002.jpeg	74200	506	459	5.3869	2.50854	8.97373	7.03405	4.95564	2.86056
27	IM-0033-0001	IM-0033-0001.jpeg	50553	414	383	3.98913	1.76931	8.28665	6.84087	5.81284	3.11669
28	IM-0035-0001	IM-0035-0001.jpeg	102719	620	582	5.4385	4.60856	12.0046	9.72945	5.42734	2.19512
29	IM-0036-0001	IM-0036-0001.jpeg	67845	524	427	1.06626	2.04726	12.4476	7.6783	6.31618	3.6289
30	IM-0037-0001	IM-0037-0001.jpeg	51648	435	376	4.10815	3.02052	9.3078	7.35064	3.8106	2.43976
31	IM-0039-0001	IM-0039-0001.jpeg	70174	538	448	3.29292	5.10041	7.83079	6.08135	5.07773	3.30292
32	IM-0041-0001	IM-0041-0001.jpeg	78511	505	517	2.85865	1.85259	7.29115	5.20013	4.42498	-0.822645
33	IM-0043-0001	IM-0043-0001.jpeg	87744	574	508	4.04308	2.47866	9.87489	7.18476	5.1064	3.02462

Fig. 5 Image Embedding

3) Dataset Details and Analysis

Chest X-Ray Images (Pneumonia) Dataset used. Contains 5,863 X-ray images, divided into Train, Test, and Validation sets
For this study, a subset of 2000 images were selected:

- 1000 Normal Chest X-rays
- 1000 Pneumonia Chest X-rays

Original images were downscaled by 4× using bicubic interpolation to create low-resolution (LR) images. The fine-tuned Real-ESRGAN model was applied to enhance the LR images, generating 1000 SR Normal and 1000 SR Pneumonia images

4) Neural network and Parameter Settings

A neural network is used as the classification model for pneumonia detection. The architecture consists of a fully connected layer with 256 neurons, ReLU activation, and the Adam optimizer. Regularization with an alpha value of 0.3 is applied to prevent overfitting. The maximum number of iterations is set to 2000 to ensure sufficient training time. The model is trained separately on LR and SR image embeddings to evaluate the impact of super-resolution on classification accuracy.

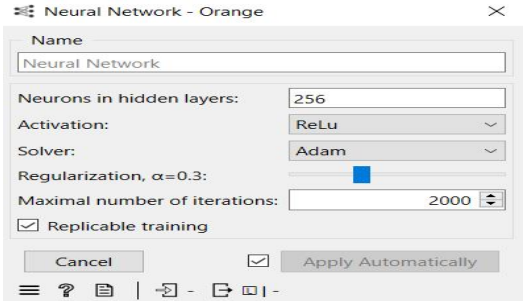

Fig. 6 Neural Network Configuration in Orange Data Mining

International Journal for Research in Applied Science & Engineering Technology (IJRASET)
ISSN: 2321-9653; IC Value: 45.98; SJ Impact Factor: 7.538
Volume 13 Issue III Mar 2025- Available at www.ijraset.com

V. RESULTS & DISCUSSION

A. Super-Resolution Model Results

1) Visual Comparison with Ground Truth

The effectiveness of the super-resolution model is comparatively visually analyzed on the basis of generated high-resolution images with their corresponding ground truth images. Side-by-side comparisons basically highlight how the model can reconstruct fine details and enhance image clarity. In addition, regions will be magnified to inspect performance in enhancing structural details, which are important for medical diagnosis.

To benchmark the super-resolution model, low-resolution (LR) images were created from high-resolution (HR) chest X-rays by downscaling their size by a factor of 4 by bicubic interpolation with light **Gaussian blur ($\sigma = 0.5$)** and **JPEG compression (quality = 70%)**, closely mimicking real-life degradation. This process is similar to quality degradation encountered in portable X-ray systems. Super-resolved images (SR) were visually compared with their corresponding ground truth (original) images to determine the model's ability to restore fine details.

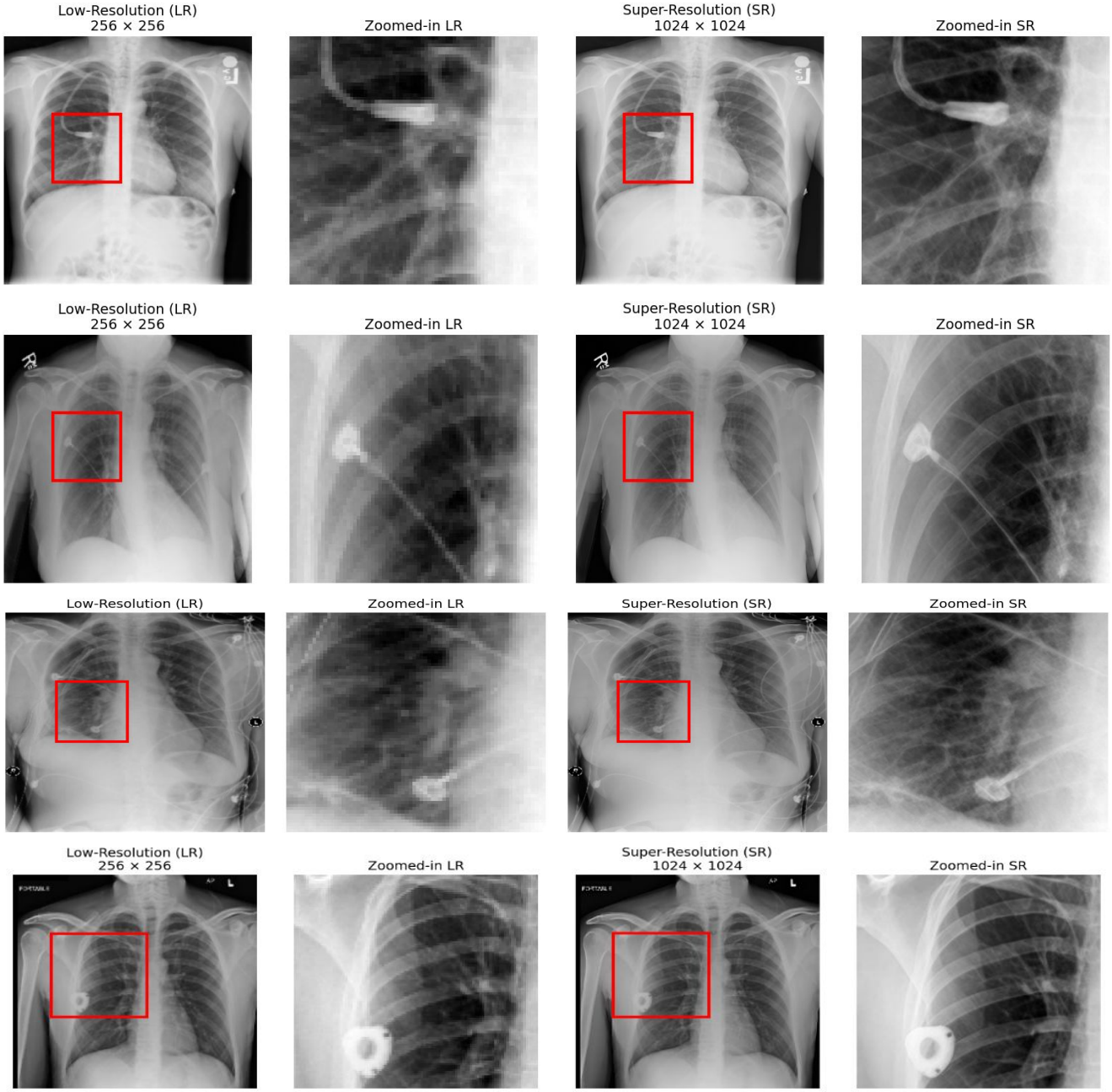

Fig 7 Visual Comparison with Ground Truth

2) Quantitative Metrics: PSNR, SSIM, and MSE

Table. 4 SR Model Performance Comparison

Metric	Dataset	Between Original & LR	Between SR & LR	Improvement (%)
PSNR	Same dataset	34.463706	36.066711	4.66%
SSIM		0.940185	0.952876	1.35%
MSE		28.383241	17.445213	-38.56%
PSNR	Unseen	34.947938	36.997566	5.86%
SSIM		0.873238	0.953419	9.19%
MSE		22.056937	13.30304	-39.67%

Above quantitative evaluation is performed using PSNR, SSIM, and MSE.

- *Peak Signal-to-Noise Ratio (PSNR)*

PSNR measures the ratio between the maximum possible power of a signal and the power of corrupting noise that affects the image quality. It is expressed in decibels (dB), where a higher PSNR indicates better image quality.

$$PSNR = 10 \cdot \log_{10}\left(\frac{MAX_I^2}{MSE}\right)$$

where:

- MAX_I is the maximum possible pixel value (e.g., 255 for an 8-bit image).
- MSE is the mean squared error between the original and reconstructed images.

- *Structural Similarity Index (SSIM)*

SSIM measures the structural similarity between two images by considering luminance, contrast, and structure. It ranges from -1 to 1, where **1** indicates identical images.

$$SSIM(x,y) = \frac{(2\mu_x\mu_y + C_1)(2\sigma_{xy} + C_2)}{(\mu_x^2 + \mu_y^2 + C_1)(\sigma_x^2 + \sigma_y^2 + C_2)}$$

where:

- μ_x, μ_y are the mean values of images x and y.
- σ_x^2, σ_y^2 are variances of images.
- σ_{xy} is the covariance.
- C_1, C_2 are small constants to avoid division by zero.

- *Mean Squared Error (MSE)*

MSE calculates the average squared difference between the original and reconstructed images. A lower MSE value indicates a higher image quality.

$$MSE = \frac{1}{MN}\sum_{i=1}^{M}\sum_{j=1}^{N}[I_{orig}(i,j) - I_{recon}(i,j)]^2$$

where:

- I_{orig} and I_{recon} are the original and reconstructed images.
- M and N are the image dimensions.

The comparison is conducted in two stages:

- Between Original & LR Images: This measures the degradation caused by downscaling, highlighting the loss of information in the low-resolution images.
- Between SR & LR Images: This evaluates how much improvement the super-resolution model provides when enhancing the low-resolution images.

The improvement percentage between the two comparisons is used to validate the effectiveness of super-resolution. A significant increase in PSNR and SSIM, along with a reduction in MSE, indicates that the model successfully reconstructs fine details and improves image quality.

Additionally, the evaluation is conducted on two datasets:

- Unseen images from the training dataset: Used to verify the model's ability to enhance images similar to those seen during training.
- Completely unseen dataset: Used to assess the robustness of the model in handling entirely new images.

The results show that super-resolution (SR) improves image quality, with PSNR and SSIM increasing while MSE decreases significantly for both the same and unseen datasets. The unseen dataset shows a higher SSIM gain (9.19%), suggesting better structural preservation. However, the moderate PSNR improvement indicates that while SR enhances clarity, it does not fully restore all details

Overall, SR positively impacts image quality, but further refinements may be needed for more consistent improvements.

B. Pneumonia Detection Model Results

The model's performance was analyzed using both low-resolution (LR) and super-resolved (SR) images as inputs and the classification model was tested using a neural network, and its performance was assessed based on accuracy, precision, recall, and F1-score MCC.

Were these metrices shows

- AUC: Measures the ability to distinguish between classes (higher is better).
- CA (Classification Accuracy): Percentage of correct predictions.
- F1 (F1-score): Harmonic mean of Precision and Recall, balancing both.
- Prec (Precision): True Positives / (True Positives + False Positives), measuring correctness of positive predictions.
- Recall: True Positives / (True Positives + False Negatives), measuring how well positives are identified.
- MCC (Matthews Correlation Coefficient): Measures overall quality of classification (balanced across classes).

The LR images for this evaluation downscaled by using bicubic interpolation without blur or JPEG compression effects by x4 scale factor. The goal was to determine whether using SR images improved pneumonia detection compared to LR images for evaluation of pneumonia classification model

1) Classification Performance on LR vs. SR Images

The pneumonia detection model was trained and then tested using low-resolution images separately from the super-resolution images to compare their classification efficiency. The evaluation done using random sampling with stratified train-test split in two various configurations:

- Train/Test Split 60% (40% test data)
- Train/Test Split 50% (50% test data)

In both configurations, the classification model was tested on 1000 normal and 1000 pneumonia images.

Table. 5 Pneumonia classification model Performance

Repeat train/test : 2 & Training set size : 60%							
Image type	Model	AUC	CA	F1	Prec	Recall	MCC
LR	Neural Network	0.98	0.932	0.932	0.932	0.932	0.864
SR		0.981	0.938	0.938	0.938	0.938	0.876
Improvement		0.10%	0.64%	0.64%	0.64%	0.64%	1.39%

Repeat train/test : 2 & Training set size : 50%							
Image type	Model	AUC	CA	F1	Prec	Recall	MCC
LR	Neural Network	0.98	0.934	0.934	0.934	0.934	0.868
SR		0.983	0.939	0.939	0.939	0.939	0.878
Improvement		0.31%	0.54%	0.54%	0.54%	0.54%	1.15%

These results achieved on 4× downscaling without adding any blur or degradation LR images the SR images still showed an improvement in pneumonia classification performance. This suggests that super-resolution enhances feature extraction even with simple downscaling.
Further test with real-world low-quality X-rays could provide deeper insights into the robustness of SR in clinical settings.

2) Confusion Matrix and Comparative Analysis

The matrices represent the proportion of actual classes (normal and pneumonia) classified correctly or misclassified. By evaluating True Positives (TP), False Positives (FP), True Negatives (TN), and False Negatives (FN), It can be determined whether the SR images helped in improving classification performance. Metrices for **LR (left)** & for **SR (right)** shown in figure. 8 & figure. 9

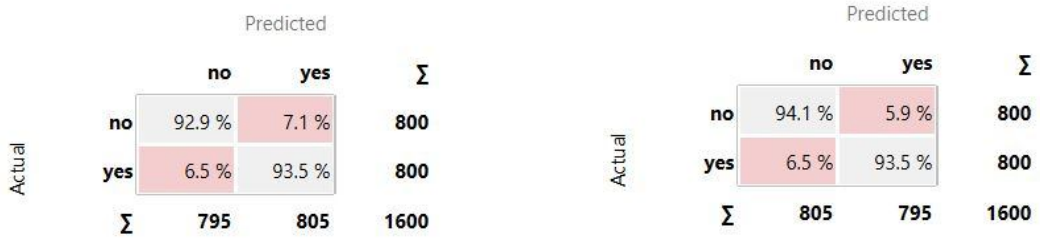

Fig. 8 For Repeat train/test : 2 & Training set size : 60%

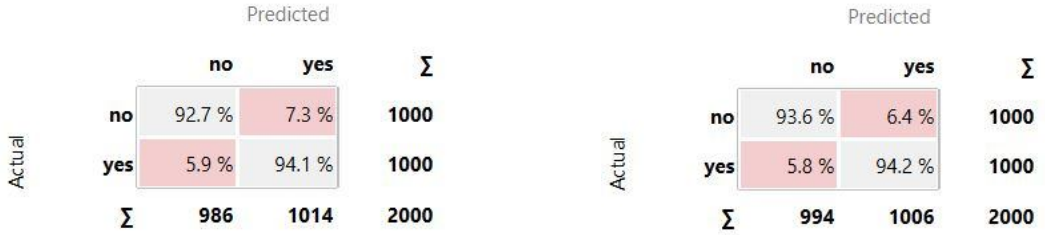

Fig. 9 For Repeat train/test : 2 & Training set size : 50%

C. Discussion

1) Limitations of the Proposed Approach

A major limitation of the suggested strategy is its high-performance graphical processing unit (GPU) dependency, requiring one to utilize cloud environments like Google Colab that are free to access with time limits. In addition, even though the dataset employed in this work is a formally published dataset by the National Institutes of Health (NIH), the real-world utility is not verified since the model is not directly trained or tested from data collected from hospitals or imaging centers. Moreover, the performance of the model may be further improved by larger-scale training iterations, more epochs, and more extreme data augmentation techniques.

2) Future work

Further research will be done to optimize the model for it to be smoothly embedded in portable X-ray cameras. Thus, the result will be real-time super-resolution enhancement for low-resolution scans captured in remote or resource-limited settings. Model deployment will be explored through cloud-based and edge AI solutions to ensure fast and efficient processing without requiring high-end local hardware. Besides, an online application or dashboard can be built to provide the features of image enhancement and the diagnosis of pneumonia with automatic programs, where doctors will be able to send and examine X-ray images remotely. The same method can be employed to other medical imaging applications, such as tuberculosis, lung cancer, and bone fracture detection, in overcoming diagnostic errors among various diseases.

VI. CONCLUSION

This study explored super-resolution for pneumonia detection in chest X-rays, showing accuracy improvement over low-resolution images on same training dataset and also for completely unseen dataset. The SR model demonstrated enhanced perceptual quality and structural details. The super-resolved (SR) images improved classification accuracy compared to low-resolution (LR) images, with the SR-based pneumonia detection model achieving higher accuracy. These findings highlight the potential of AI-driven super-resolution in medical imaging and enabling cost-effective diagnostics.

REFERENCES

[1] Yue, L., Shen, H., Li, J., Yuan, Q., Zhang, H., & Zhang, L. (2016). Image super-resolution: The techniques, applications, and future. Signal Processing, 128, 389–408. https://doi.org/10.1016/j.sigpro.2016.05.002
[2] Fritsche, M., Gu, S., & Timofte, R. (2019). Frequency separation for real-world super-resolution. In Proceedings of the IEEE/CVF International Conference on Computer Vision Workshops (pp. 3599–3608).
[3] Nijhawan, R., Verma, R., Bhushan, S., Dua, R., & Mittal, A. (2017). An integrated deep learning framework approach for nail disease identification. In 2017 13th International Conference on Signal-Image Technology & Internet-Based Systems (SITIS) (pp. 197–202). IEEE. https://doi.org/10.1109/SITIS.2017.41
[4] C. Ledig, L. Theis, F. Huszár, J. Caballero, A. Cunningham, A. Acosta, A. Aitken, A. Tejani, J. Totz, Z. Wang, et al., "Photorealistic single image super-resolution using a generative adversarial network," arXiv preprint, 2016.
[5] Y. Zhang, Y. Tian, Y. Kong, B. Zhong, Y. Fu, "Residual dense network for image super-resolution," in The IEEE Conference on Computer Vision and Pattern Recognition (CVPR), 2018.
[6] Dawit Kiros Redie, Abdulhakim Edao Sirko, Tensaie Melkamu Demissie, Semagn Sisay Teferi, Vimal Kumar Shrivastava, Om Prakash Verma, Tarun Kumar Sharma, Diagnosis of COVID-19 using chest X-ray images based on modified DarkCovidNet model, Evol. Intell. 16 (3) (2023) 729–738.
[7] Yibo Feng, Xu Yang, Dawei Qiu, Huan Zhang, Dejian Wei, Jing Liu, Pcxrnet: pneumonia diagnosis from chest x-ray images using condense attention block and multiconvolution attention block, IEEE J. Biomed. Health Inform. 26 (4) (2022) 1484–1495.
[8] Y. Li, Bruno Sixou, F. Peyrin, A review of the deep learning methods for medical images super-resolution problems, Irbm 42 (2) (2021) 120–133.
[9] Jing Tian, Kai-Kuang Ma, A survey on super-resolution imaging, Signal. Image Video Process. 5 (2011) 329–342.
[10] Hujun Yang, Zhongyang Wang, Xinyao Liu, Chuangang Li, Junchang Xin, Zhiqiong Wang, Deep learning in medical image super resolution: a review, Appl. Intell. (2023) 1–26.
[11] I. Sirazitdinov, M. Kholiavchenko, T. Mustafaev, Y. Yixuan, R. Kuleev, and B. Ibragimov, "Deep neural network ensemble for pneumonia localization from a large-scale chest x-ray database," Computers & Electrical Engineering, vol. 78, pp. 388-399, 2019.
[12] K. Hammoudi et al., "Deep Learning on Chest X-ray Images to Detect and Evaluate Pneumonia Cases at the Era of COVID-19," arXiv preprint arXiv:2004.03399, 2020.
[13] A. K. Jaiswal, P. Tiwari, S. Kumar, D. Gupta, A. Khanna, and J. J. Rodrigues, "Identtifying pneumonia in chest X-rays: A deep learning approach," Measurement, vol. 145, pp. 511-518, 2019.
[14] C. Dong, C. C. Loy, K. He, and X. Tang, “Image super-resolution using deep convolutional networks,” IEEE Transactions on Pattern Analysis and Machine Intelligence, vol. 38, no. 2, pp. 295–307, Feb. 2016, doi: 10.1109/TPAMI.2015.2439281.
[15] L. Xu, X. Zeng, Z. Huang, W. Li, and H. Zhang, “Low-dose chest X-ray image super-resolution using generative adversarial nets with spectral normalization,” Biomedical Signal Processing and Control, vol. 55, p. 101600, Jan. 2020, doi: 10.1016/j.bspc.2019.101600.
[16] A. Khishigdelger, A. Salem, and H. S. Kang, “Elevating chest X-ray image super-resolution with residual network enhancement,” Journal of Imaging, vol. 10, no. 3, p. 64, Mar. 2024, doi: 10.3390/jimaging10030064.
[17] K. Ahmadian and H. R. Alikhani, “X-ray medical image super-resolution via self-organization neural networks and geometric directional gradient,” IET Image Processing, vol. 16, no. 14, pp. 3910–3928, Dec. 2022, doi: 10.1049/ipr2.12603.
[18] A. Mittal et al., “Detecting pneumonia using convolutions and dynamic capsule routing for chest X-ray images,” Sensors (Switzerland), vol. 20, no. 4, pp. 1–30, 2020, doi: 10.3390/s20041068.
[19] B. Imran and L. D. Bakti, “Implementation of Machine Learning Model for Pneumonia Classification Based on X-Ray Images,” J. Mantik, vol. 5, no. 3, pp. 2101–2107, 2021.
[20] K. R. Swetha, M. Niranjanamurthy, M. P. Amulya, and M. Y. Manu, “Prediction of Pneumonia Using Big Data, Deep Learning and Machine Learning Techniques,” Proc. 6th Int. Conf. Commun. Electron. Syst. ICCES 2021, no. August, pp. 1697–1700, 2021, doi: 10.1109/ICCES51350.2021.9489188.
[21] X. Wang, L. Xie, C. Dong, and Y. Shan, “Real-ESRGAN: Training real-world blind super-resolution with pure synthetic data,” arXiv preprint arXiv:2107.10833, 2021. Available: https://arxiv.org/abs/2107.10833.
[22] C. Dong, C. C. Loy, K. He, and X. Tang, “Image super-resolution using deep convolutional networks,” IEEE Transactions on Pattern Analysis and Machine Intelligence, vol. 38, no. 2, pp. 295–307, 2016. doi: 10.1109/TPAMI.2015.2439281.
[23] X. Wang, Y. Yu, K. Gu, S. Wu, J. Gu, C. Dong, Y. Qiao, and C. C. Loy, “ESRGAN: Enhanced super-resolution generative adversarial networks,” in Proceedings of the European Conference on Computer Vision (ECCV) Workshops, 2018. Available: https://arxiv.org/abs/1809.00219.
[24] Moneebah. (n.d.). GitHub - Moneebah/Finetuning_Real-ESRGAN_Pneumonia: Finetuning pretrained model of Real-ESRGAN onto chest xrays (with and without pneumonia). GitHub. https://github.com/Moneebah/Finetuning_Real-ESRGAN_Pneumonia
[25] Random sample of NIH Chest X-ray Dataset. (2017, November 23). Kaggle. https://www.kaggle.com/datasets/nih-chest-xrays/sample
[26] Chest X-Ray images (Pneumonia). (2018, March 24). Kaggle. https://www.kaggle.com/datasets/paultimothymooney/chest-xray-pneumonia

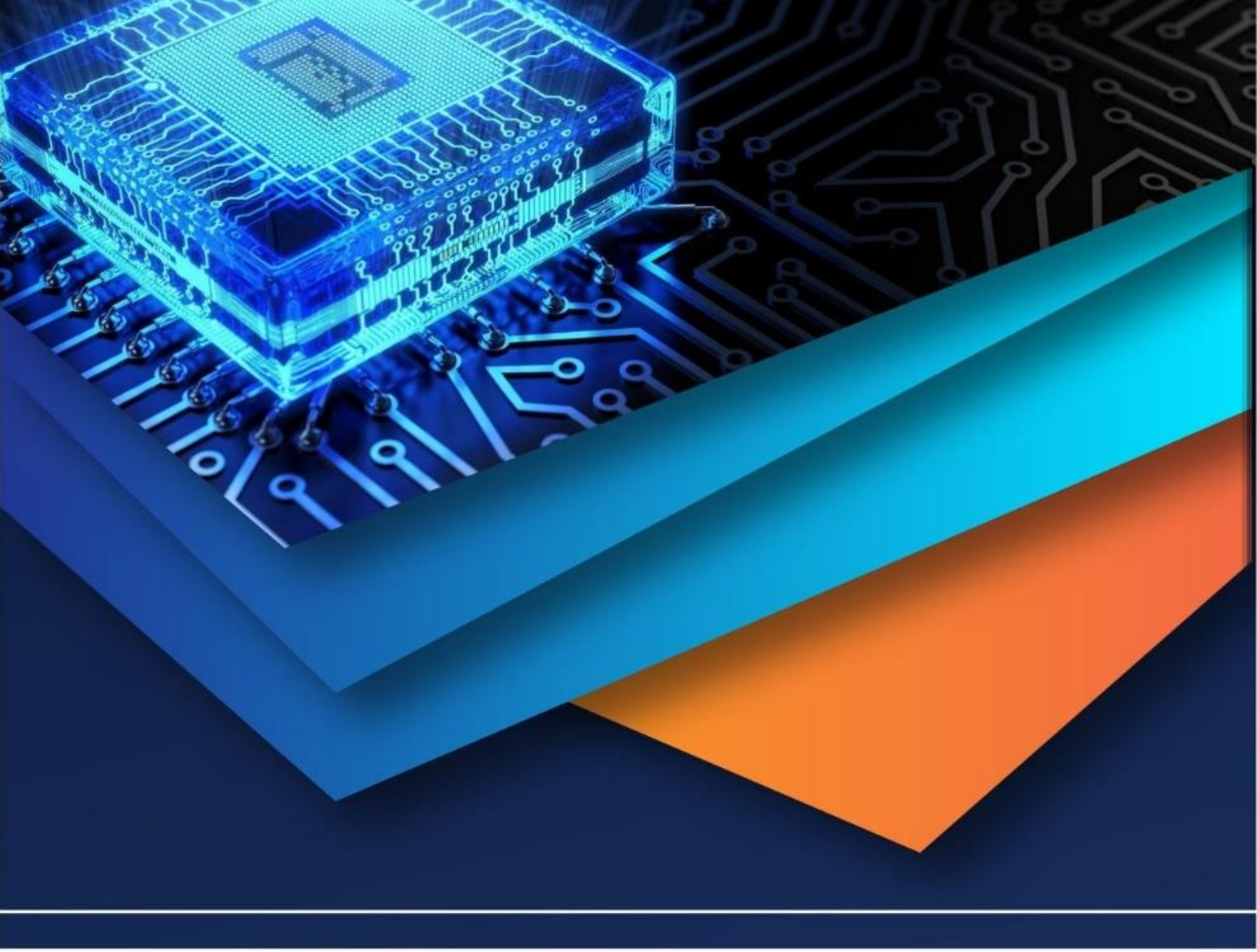

10.22214/IJRASET

45.98

IMPACT FACTOR: 7.129

IMPACT FACTOR: 7.429

INTERNATIONAL JOURNAL FOR RESEARCH

IN APPLIED SCIENCE & ENGINEERING TECHNOLOGY